Appl. Sci. Converg. Technol. 25(2): 36-41 (2016)
http://dx.doi.org/10.5757/ASCT.2016.25.2.36

Research Paper

Various Quantum Ring Structures: Similarity and diversity

Dae-Han Park and Nammee Kim*
Department of Physics, Soongsil University, Seoul 06978, Korea

Received February 22, 2016; accepted March 4, 2016

Abstract Similarity and diversity of various quantum ring structures are investigated by classifying energy dispersions of three different structures: an electrostatic quantum ring, a magnetic quantum ring, and a magnetic-electric quantum ring. The wave functions and the eigenenergies of a single electron in the quantum ring structures are calculated by solving the Schrdinger equation without any electron-electron interaction. Magnetoconductance is studied by calculating a two-terminal conductance while taking into account the backscattering via the resonance through the states of the quantum rings at the center of a quasi-one dimensional conductor. It is found that the energy spectra for the various quantum ring structures are sensitive to additional electrostatic potentials as well as to the effects of a nonuniform magnetic field. There are also characteristics of similarity and diversity in the energy dispersions and in the single-channel magnetoconductance.

Keyword: Single particle states, Electronic transport, Hybrid Quantum Structure, Magnetoconductance

I. Introduction

For the last several decades, there has been a great deal of interest in various magnetically confined quantum structures such as a magnetic quantum dot formed using a scanning tunneling microscope lithographic technique, [1] a magnetic antidot, a magnetic quantum ring formed by spatially inhomogeneous magnetic fields in a two dimensional electron gas (2DEG), and magnetic superlattices formed using a patterning of ferromagnetic materials integrated in a semiconductor [2]. Recently, the study of 2DEG-based magnetic quantum structures has expanded to graphene-based quantum structures [3-5].

Theoretical developments have focused on the energy spectra of electrons confined in these magnetic quantum structures [6,7]. Those structures have current-carrying states, existing along the boundary between two different magnetic domains; these are the so-called the magnetic edge states. These magnetic structures are analogous to conventional quantum structures confined by electrostatic potentials, but they show transport properties distinct from those of conventional structures due to their characteristic electronic structures. [6-9] One of these magnetic quantum structures, the electronic structure of a magnetic quantum ring, has previously been investigated by the author's group [10]. In the Quantum Hall regime, electronic transport through a quasi-one-dimensional (1D) wire in the presence of an external magnetic field can be well described in terms of the edge-state picture. The transport properties of the quasi-1 wire show quantized magnetoconductance and resonant tunneling behaviors when edge channels are scattered by local electrostatic modulation, i.e., by electrostatic antidot potential, [11] or by local magnetic modulation such as a magnetic quantum dot [7] and a magnetic quantum ring [12].

In this paper, we present an in-depth pedagogical study on three different kinds of quantum ring structures: an electrostatic quantum ring (EQR) with an uniform magnetic field, a magnetic quantum ring (MQR) formed by spatially inhomogeneous magnetic fields in 2DEG, and a magnetic-electric quantum ring (MEQR) formed by a magnetic quantum dot combined with an additional antidot electrostatic potential at the center of the dot. In previous works, there has been no attempt to characterize the properties of the three kinds of quantum ring structures at the same time and study of the aspects of electron transport, such as the magnetoconductance, has often been left out. It should be noted that the conductance calculation involves a great deal of numerical works to obtain the energy eigenvalues, while these values can be obtained analytically for a conventional electrostatic quantum ring structure. Previous studies have looked at the energy dispersion for MQR [10]; however, in this work we additionally and in detail show the similarity and diversity of energy dispersion using a comparison of the results of EQR and MEQR. We calculate the magnetoconductance behaviors of the three different quantum rings in the same way that we study the magnetoconductance of a quantum dot [7] and of a magnetic quantum ring [12]. We discuss

*Corresponding author
E-mail: nammee@ssu.ac.kr

the characteristics of similarity and diversity in magnetoconductance among the three different quantum rings: EQR, MQR, and MEQR.

II. The Single Particle Schrödinger Equation and Wave Functions

The general form of the single-particle Schrödinger equation for various quantum ring structures without electron-electron interaction is written as

$$\left\{\frac{1}{2m^*}(\vec{P}+e\vec{A})^2+V(r)\right\}\varphi(\vec{r})=E\varphi(\vec{r}). \quad (1)$$

Here, e is the magnitude of an electron charge, $\vec{A}$ is the vector potential, and V(r) is the electrostatic potential. In our calculation, the vector potential $\vec{A}$ can be chosen to have a symmetric gauge (Coulomb gauge) with a A_θ component only, in plane polar coordinates (r, θ). $\vec{P}$ is the momentum operator. We have solved this single-particle Schrdinger equation in the plane polar coordinates (r, θ). The wave function can be written in a separable form as $\varphi(\vec{r}) = R_{nm}(r)e^{im\theta}$, where m is the angular momentum quantum number and n (=0, 1, 2...) is the number of nodes in the radial wave function. After eliminating in Eq. (1), the equation of the radial part is written as

$$\left\{\frac{d^2}{dr^2}+\frac{1}{r}+\frac{d}{dr}+\frac{2m^*}{\hbar^2}(E_{nm}-V_{eff}(r))\right\}R_{nm}(r)=0, \quad (2)$$

where

$$V_{eff}(r)=V(r)+\frac{\hbar^2}{2m^*}\left(\frac{m^2}{r^2}+\frac{2meA_\theta}{r\hbar}+\frac{e^2|A_\theta|^2}{\hbar^2}\right), \quad (3)$$

and the equation of the radial part is simplified in dimensionless units as,

$$\left\{\frac{d^2}{d\rho^2}+\frac{1}{\rho}+\frac{d}{d\rho}+2(\varepsilon_{nm}-V_{eff}(\rho))\right\}R_{nm}(\rho)=0, \quad (4)$$

where $\rho = \beta r$, $\varepsilon_{nm} = E_{nm}/\hbar\omega_0$. The effective potential V_{eff}(r) is defined differently for each quantum ring structure depending on the given V(r) and A_θ. β is the characteristic wave number to make r a dimensionless variable. All quantities are expressed in dimensionless units by letting $\hbar\omega_0\left(=\frac{\hbar eB_0}{2m^*}\right)$ and the inverse length $\beta(=\sqrt{m^*\omega_0/\hbar})$ be 1. Therefore, we use r instead of using ρ in Eq. (4) from now on. While the cyclotron frequency for the external magnetic field B_0 is $\omega_c = \frac{eB_0}{m^*}$, we define the standard frequency $\omega_c = \frac{eB_0}{2m^*}$ for an easy expression of electrostatic potentials in the familiar way. In these units, $\hbar/m^* = \hbar\omega_0/\beta^2 \to 1$. ω_0 is the standard frequency in units of energy. By solving Eq. (4), we can obtain the wavefunction of each quantum ring with the given geometric properties and the vector potential $\vec{A}$ and the additional electrostatic potential $V(r)$.

1. An electrostatic quantum ring (EQR)

An EQR is formed in 2DEG with a uniform magnetic field ($\vec{B} = B\hat{z}$), with the electrostatic potential written as

$$V(r)=\frac{\delta}{2r^2}m^*\omega_0{}^2r_0{}^4+\frac{1}{2}m^*\alpha^2\omega_0{}^2r^2. \quad (5)$$

Here, m* is the effective mass of an electron. δ and α are parameters that describe the strengths of the antidot and the parabolic potential, respectively. r_0 is a parameter that describes the size of EQR with δ and α.

For the uniform external magnetic field, the vector potential $\vec{A}$ in Eq. (1) can be chosen to have a symmetric gauge (Coulomb gauge) as $\vec{A} = \frac{1}{2}Br\hat{\theta} = \frac{1}{2}\gamma Br\hat{\theta}$ in plane polar coordinates (r, θ); $\gamma = \frac{B}{B_0}(\gamma > 0)$ is the ratio of the applied external magnetic field to the standard magnetic field The effective potential $V_{eff}(r)$ is obtained by substituting and $V(r)$ into Eq. (3) and is expressed in dimensionless units as

$$V_{eff}(r)=\frac{m^2+\delta s_0{}^2}{2r^2}+\frac{1}{2}(\gamma^2+\alpha^2)r^2+\gamma m, \quad (6)$$

where $s_0 = \frac{\pi r_0{}^2B_0}{\phi_0}$ defines the magnetic flux in a circle with the radius r_0. In dimensionless units, $r_0 \to \sqrt{s_0}$.

The wave functions $R_{nm}(r)$ are calculated from Eq. (4) and written as

$$R_{nm}(\mathrm{r})=C_1(\sqrt{\gamma^2+\alpha^2}r)^{\sqrt{m^2+\delta s_0{}^2}}e^{-\frac{1}{2}\sqrt{\gamma^2+\alpha^2+r^2}} \quad (r>r_0)$$

$$a_1=-\frac{1}{2}\left(\frac{\varepsilon_{nm}}{\sqrt{r^2+\alpha^2}}-\frac{rm}{\sqrt{r^2+\alpha^2}}-\sqrt{m^2+\delta s_0{}^2-1}\right) \quad (7)$$

$$b_1=\sqrt{m^2+\delta s_0{}^2}+1,$$

where U is the confluent hypergeometric function.

2. A magnetic quantum ring (MQR)

A MQR is formed by the nonuniform magnetic field; $B \neq 0$ for $r < r_1$, $B = 0$ for $r_1 < r < r_2$, and $B \neq 0$ for $r > r_2$. The direction of the magnetic field is perpendicular to the 2DEG. In this quantum structure, we do not have the additional electrostatic potential V(r). We consider the same magnetic field strength for $r < r_1$, and $r > r_2$ in this work. In plane polar coordinates (r, θ) is in the plane, and the vector potential $\vec{A}$ can be chosen to have a symmetric gauge as in [10]:

$$\vec{A}=\hat{\theta}\begin{cases}\frac{1}{2}\gamma B_0 r & (r<r_1)\\ \frac{1}{2r}\gamma B_0 r_1{}^2 & (r_1<r<r_2)\\ \frac{1}{2}\gamma B_0 r-\frac{1}{2r}\gamma B_0(r_2{}^2-r_1{}^2) & (r<r_1),\end{cases} \quad (8)$$

$\gamma = \frac{B}{B_0}$ is the ratio of the applied external magnetic field to the standard magnetic field B_0.

The effective potential $V_{eff}(r)$ with $V(r) = 0$ is then

written as

$$V_{eff}=\begin{cases}\frac{1}{2}\gamma^2 r^2+\frac{m^2}{2r^2}+\gamma m_{eff,1} & ,m_{eff,1}=m \quad (r<r_1)\\ \frac{m_{eff,2}^2}{2r^2} & ,m_{eff,2}=m+\gamma s_1 \quad (r_1<r<r_2)\\ \frac{1}{2}\gamma^2 r^2+\frac{m_{eff,3}^2}{2r^2}+\gamma m_{eff,3} & ,m_{eff,3}=m+\gamma(s_2-s_1)\ (r_2<r_1),\end{cases} \tag{9}$$

where $s_1 = \pi r_1^2 B_0/\phi_0$ and $s_2 = \pi r_2^2 B_0/\phi_0$ and $\phi_0\left(=\frac{h}{e}\right)$ is the flux quantum.

$$R_{nm}(r)=\begin{cases}C_2(\gamma r)^{|m_{eff,1}|}e^{-\frac{1}{2}\gamma r^2}M(a_2,b_2;\gamma r^2) & (r<r_1)\\ C_3 J_{|m_{eff,2}|}(\sqrt{2\varepsilon_{nm}}r)+C_4 N_{|m_{eff,2}|}(\sqrt{2\varepsilon_{nm}}r) & (r_1<r<r_2)\\ C_5(\gamma r)^{|m_{eff,3}|}e^{-\frac{1}{2}\gamma r^2}U(a_3,b_3;\gamma r^2) & (r_2<r),\end{cases} \tag{10}$$

where $a_2 = \left(\frac{1}{2}|m_{eff,1}|+1-\frac{\varepsilon_{nm}}{\gamma}+m_{eff,1}\right)$, $b_2 = |m_{eff,1}|+1$, $a_3 = \left(\frac{1}{2}|m_{eff,3}|+1-\frac{\varepsilon_{nm}}{\gamma}+m_{eff,3}\right)$, and $b_3 = |m_{eff,3}|+1$. Functions J and N are the Bessel functions and M and U are the confluent hypergeometric functions. The expression in Eq. (9) and Eq. (10) are different from Ref. [10] because, when we define dimensionless units in this work, we use B_0 as a standard magnetic field, while we used the external magnetic field B itself as the standard magnetic field in previous work.

3. Magnetic-electric quantum ring (MEQR)

A MEQR is formed by the combination of an electrostatic potential and a nonuniform magnetic field. We introduce an additional antidot electrostatic potential $V(r) = \frac{\delta}{2r^2}m^*\omega_0^2 r_0^4$ at the center of a magnetic dot having the radius r_0 $\vec{B} = 0$ for $r < r_0$ and $\vec{B} = B\hat{z}$, elsewhere. Here, δ is a parameter that describes the strength of the antidot potential which repels electron away from the dot center.

In plane polar coordinates (r, θ), the vectosr potential $\vec{A}$ can be chosen to have a symmetric gauge as

$$\vec{A}=\hat{\theta}\begin{cases}0 & (r<r_0)\\ \frac{1}{2}\gamma B_0 r-\frac{1}{2r}\gamma B_0 r_0^2 & (r>r_0)\end{cases} \tag{11}$$

The effective potential V_{eff} is expressed as:

$$V_{eff}=\begin{cases}\frac{m^2+\delta s_0^2}{2r^2} & (r<r_0)\\ \frac{m_{eff}^2+\delta s_0^2}{2r^2}+\frac{1}{2}\gamma^2 r^2+\gamma m_{eff} & (r>r_0),\end{cases} \tag{12}$$

where $m_{eff} = m - \gamma s_0$, $s_0 = \pi r_0^2 B_0/\phi_0$.

The wave functions are expressed by the Bessel function J and the confluent hypergeometric function U as:

$$R_{nm}(r)=\begin{cases}C_6 J_{\sqrt{m^2+\delta s_0^2}}(\sqrt{2\varepsilon_{nm}}r) & (r<r_0)\\ C_7(\gamma r)^{\sqrt{m_{eff}^2+\delta s_0^2}}e^{-\frac{1}{2}\gamma r^2}U(a_4,b_4;\gamma r^2) & (r>r_0),\end{cases} \tag{13}$$

where $a_4 = -\frac{1}{2}\left(\frac{\varepsilon_{nm}}{\gamma}-m_{eff}-\sqrt{m_{eff}^2+\delta s_0^2}-1\right)$, $b_4 = \sqrt{m_{eff}^2+\delta s_0^2}+1$. Electrons confined in the magnetic quantum dot are repelled by the antidot potential. When the parameter δ is small enough that the size of the antidot is smaller than that of the magnetic quantum dot, this structure acts in a manner similar to that of a quantum ring, we call this structure MEQR.

III. Results and Discussion

1. Energy dispersion

While the eigenenergies of MQR and MEQR are determined numerically by the continuity of the wavefunctions and their derivatives at the boundaries, the eigenenergies of EQR are calculated analytically. For EQR, by substituting Eq. (7) into Eq. (4) the eigenenergies can be derived as:

$$E_{nm} = \hbar\omega_0\left\{rm+\sqrt{r^2+a^2}(2n+\sqrt{m^2+\delta s_0^2}+1)\right\}.$$

Figure 1 shows the energy dispersions of the three different quantum ring structures as a function of γ. On the y-axis, $\varepsilon_{nm} = E_{nm}/\hbar\omega_0$. Here, we plot ($n$, m): n = 0, 1, and m = –5, –4, –3, –2, –1, 0, 1, 2 for simplicity. The parameters α = 0.1, δ = 0.2 and $r_0 = \sqrt{7}$ are used for EQR (Fig. 1(a)) and $r_0 = r_2 = \sqrt{7}$, $r_1 = \sqrt{3}$, and δ = 0.2 are used for MQR (Fig. 1(b)) and MEQR (Fig. 1(c)).

In Fig. 1(a), the angular momentum transition as a function of the magnetic field can be observed. It is a well-known phenomenon in a conventional quantum ring to have a finite width confined by electrostatic potentials [13]. However in a conventional quantum dot confined by electrostatic potentials, this type of angular momentum transition in the ground state can occur only when the electron-electron interaction is included. [14] The energy dispersions shown in Fig. 1(b) (MQR) and Fig. 1(c) (MEQR) also show the existence of the angular momentum transition in the ground state without the electron-electron interaction, similar to the case of EQR. Besides the similarity of the angular momentum transition, the total shapes of the energy dispersion look different. First of all, EQR has a nonzero eigenenergy at γ = 0, while MQR (Fig. 1(b)) and MEQR (Fig. 1(c)) have zero value of ε_{nm}. This difference can be understood in the following way. While EQM has a parabolic confinement due to the parameter α, the MQR and MEQR structures have no parabolic confinement, as can be seen in Eq. (9) and Eq.

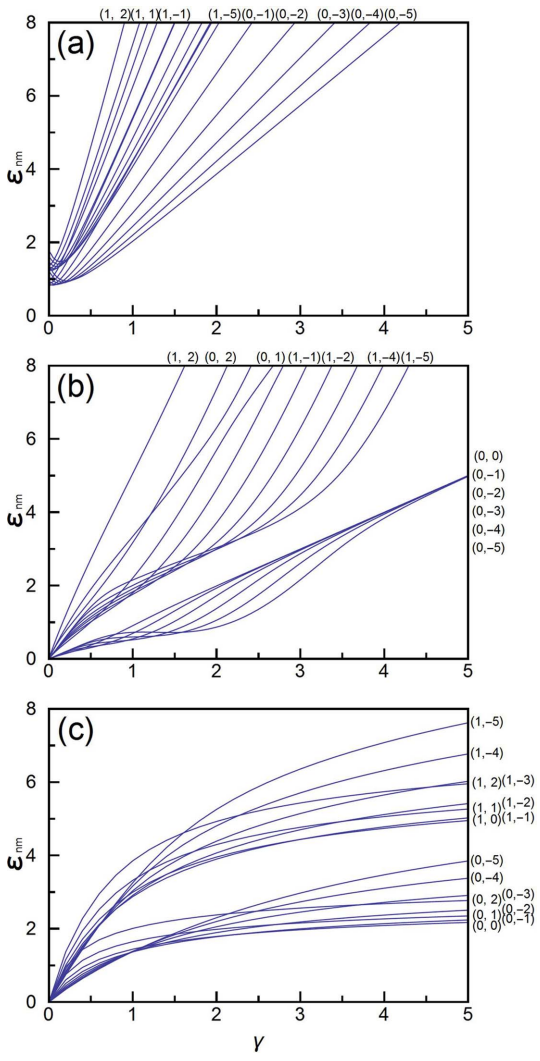

Figure 1. Eigenenergies for the states (*n, m*); $n = 0$, 1, and $m = -5, -4, -3, -2, -1, 0, 1, 2$ of as a function of γ for (a) EQR, (b) MQR, and (c) MEQR with $r_0 = r_2 = \sqrt{7}$, $r_1 = \sqrt{3}$, $\alpha = 0.1$, and $\delta = 0.2$ in dimensionless units.

(12) at $\gamma = 0$. MQR is the same as 2DEG with no external magnetic field and MEQR is the same as 2DEG having the antidot electrostatic potential. For both cases, there is no confined electron.

As can be seen in Fig. 1(b), when B is weak, (0, m) states with $m<0$ are distributed far away from the ring region to include $|m|$ amount of magnetic flux quanta and have Landau level energies. The low magnetic field means that the density of the magnetic flux is low over the ring. When B increases, states approach the ring area because of the high magnetic flux density. As the states get closer to the ring, the energies deviate from the Landau level because of the inhomogeneous distribution of the magnetic field. When B is so strong that states $m<0$ can locate within the inner circle, energies again approach the Landau level. This behavior is clearly shown between $\gamma = 0$ and $\gamma = 4.0$.

In Fig. 1(c), when B is weak, electrons feel magnetic flux missing as in the case in MQR; (0, m) states with $m<0$ are distributed far away from the dot region, where the electron feels less antidot repulsion. If the magnetic field is strong enough, the effect of the magnetic inhomogeneity becomes a dominant factor and the strong magnetic field confines the electrons nearer the center. However the states $m<0$ cannot locate within the dot due to the repulsion from the antidot potential. Therefore, energies cannot approach the Landau level in the strong magnetic field region.

II. Effective Potential and Probability Density

Figure 2 shows the effective potential $V_{eff}(r)$ and corresponding probability densities $|R_{nm}(r)|^2$ of the lowest energy state at $\gamma = 1.5$. The states (n, m) = (0, –11), (0, –4), and (0, –1) are chosen as the lowest energy eigenvalues, as can be seen Fig. 1, for EQR, MQR, and MEQR, respectively. For EQR, (n, m) = (0, –11) does not appear in Fig. 1(a), because we have plotted up to the $m = -5$ state only. We obtain (n, m) = (0, –11) directly from the minimum of $E_{nm} = \hbar\omega_0\{\gamma m + \sqrt{r^2 + a^2}(2n + \sqrt{m^2 + \delta s_0^2} + 1)\}$ with parameters $\gamma = 1.5$, $\alpha = 0.1$ $\delta = 0.2$, and $s_0 = 7$. For a certain magnetic field strength, the shape of $V_{eff}(r)$ can be controlled by changing parameters such as α and δ in Fig. 2(a) and Fig. 2(e). However, $V_{eff}(r)$ in Fig. 2(c) is fixed unless we change the size of the inner and outer radii of the ring because there is no electrostatic potential depending on α and δ in MQR. The dotted lines indicate the position of $r_0 = r_2 = \sqrt{7}$. Fig. 2(b), Fig. 2(d), and Fig. 2(f) show that an electron in the bottom state of each quantum

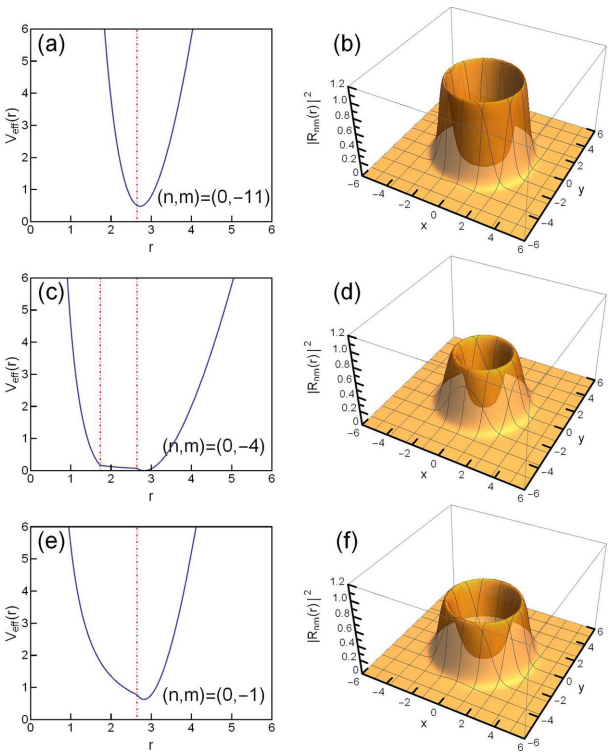

Figure 2. Effective potential $V_{eff}(r)$ and corresponding probability densities $|R_{nm}(r)|^2$ of the lowest state at $\gamma = 1.5$ for (a) EQR, (b) MQR, and (c) MEQR with $r_0 = r_2 = \sqrt{7}$, $r_1 = \sqrt{3}$, $\alpha = 0.1$, and $\delta = 0.2$ in dimensionless units.

structure stays in a ring shaped region, even though the three different rings are formed in different ways.

III. Magnetoconductance

The transport properties of the quasi-1D wire show quantized magnetoconductance. However, when edge channels are scattered by a local electrostatic modulation or magnetic modulation, the magnetoconductance shows resonant tunneling behavior. In order to investigate the resonant backscattering phenomena, we consider a quasi-1D conductor with the three different quantum rings at the center, one by one. As can be seen in Fig. 2, electron probability densities of the three different rings have ring shapes. We have determined that the width of the quasi-1D conductor is four times wider than the outer radius of the magnetic quantum ring. If the probability densities of the resonant energies stay outside of the 1D-conductor, these states are excluded in the calculation. The two-terminal conductance is calculated by the following equation as:

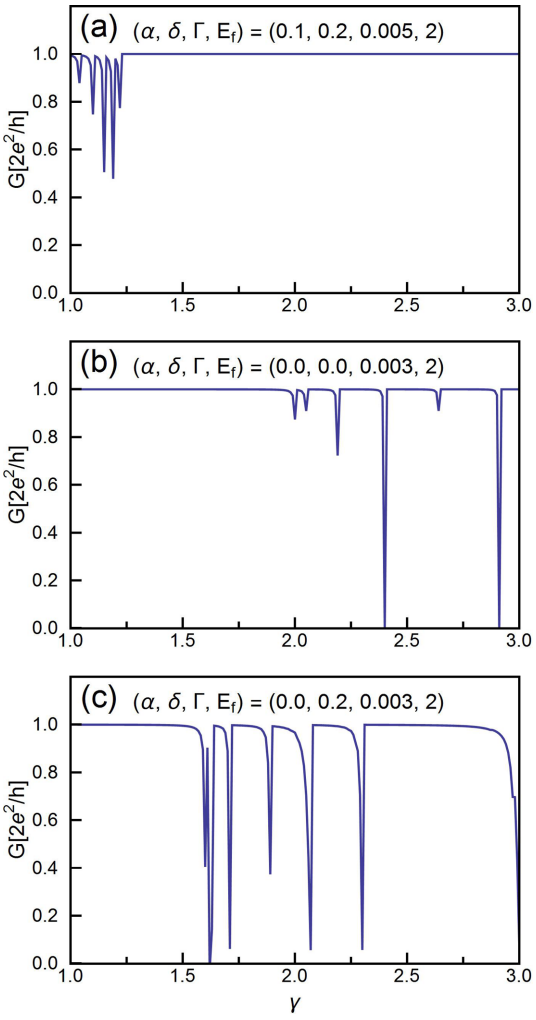

Figure 3. Magnetoconductance as a function of γ at $E_F = 2$ for (a) EQR, (b) MQR, and (c) MEQR with $r_0 = r_2 = \sqrt{7}$, $r_1 = \sqrt{3}$, $\alpha = 0.1$, and $\delta = 0.2$ in dimensionless units.

$$G(\gamma) = \frac{2e^2}{h}\left[1 - \sum_{nm} \frac{\Gamma^2}{[E_F - E_{nm}(\gamma)]^2 + \Gamma^2}\right], \quad (14)$$

where E_F is the Fermi energy and Γ is the elastic resonance width.

Figure 3 shows the results for two-terminal ballistic conductance as a function of the magnetic field γ. The parameters $r_0 = r_2 = \sqrt{7}$, $r_1 = \sqrt{3}$, $\alpha = 0.1$ and $\delta = 0.2$ are in dimensionless units. Because $\sum_{nm} \frac{\Gamma^2}{[E_F - E_{nm}(\gamma)]^2 + \Gamma^2}$ is the total transmittance by resonance through the states of the quantum rings, we can count the number of resonant peaks in Fig. 1. For EQM, as can be seen in Fig. 3(a), there are a higher number of resonant peaks between $\gamma = 1.0$ and $\gamma = 3.0$ than can be counted in Fig. 1(a); it is because we have plotted up to $m = -5$ only in this case. Because we are interested in one channel transport only, the $n = 0$ state alone is considered in the calculation. If we consider $n = 1$ and higher quantum numbers, there must be additional peaks having minus values around $\gamma = 1.0$ in Fig. 3(b). Thus we consider $E_F = 2.0$ for one channel transport instead of choosing a higher Fermi energy. All rings exhibit aperiodic fluctuation in conductance. Different from Fig. 3(b) (MQR) and Fig. 3(c) (MEQR), Fig. 3(a) (EQR) shows periodic oscillation.

IV. Conclusions

We present a pedagogic study on the electronic properties of various quantum ring structures: an electrostatic quantum ring, a magnetic quantum ring, and a magnetic-electric quantum ring. We investigate the similarity and diversity of the three different quantum ring structures by calculating the wave functions and the eigenenergies of a single electron and the single channel magnetoconductance. It is found that the energy spectra for the various quantum ring structures are sensitive to the additional electrostatic potentials, as well as to the effects of a nonuniform magnetic field. The probability densities of the electrons in the bottom state of each quantum structure have ring shapes, even though the three different quantum structures have different formation methods. All rings exhibit aperiodic fluctuation in conductance and among the three quantum rings, only the electrostatic quantum ring shows periodic oscillation. Magnetic nonuniformity has the effect of breaking the periodic oscillation of the two-terminal conductance.

Acknowledgements

This research was supported by the Basic Science Research Program through the National Research Foundation of Korea (NRF) (NRF-2015R 1D 1A 1A01058031).

References

[1] M. A. McCord and D. D. Awschalom, Appl. Phys. Lett. 57, 2153 (1990).
[2] M. L. Leadbeater, S. J. Allen, Jr., F. DeRosa, J. P. Harbison, T. Sands, R. Ramesh, L. T. Florez, and V. G. Keramidas, J. Appl. Phys. 69, 4689 (1991).
[3] S. H. Park and H. -S. Sim, Phys. Rev. B 77, 075433 (2008).
[4] C.M. Lee, R. C.H. Lee, W.Y. Ruan, M.Y. Chou, and A. Vyas, Solid State Commun. 156, 49 (2013); C. M. Lee and K. S. Chan, J. Appl. Phys. 114, 143708 (2013).
[5] Dali Wang and Guojun Jin, Phys. Lett. A 373, 4082 (2009).
[6] F. M. Peeters and A. Matulis, Phys. Rev. B 48, 15166 (1993); Phys. Rev. Lett. 72, 1518 (1994); I. S. Ibrahim and F. M. Peeters, Phys. Rev. B 52, 17321 (1995); Phys. Rev. B 56, 7508 (1997).
[7] H-S. Sim, K-H. Ahn, K. J. Chang, G.Ihm, N. Kim, and S. J. Lee, Phys. Rev. Lett. 80, 1501 (1998); H. -S. Sim, G. Ihm, N, Kim, S. J. Lee, and K. J. Chang, Physica E, 12, 719 (2002).
[8] J. E. Müller, Phys. Rev. Lett. 68, 385 (1992).
[9] M. Calvo, Phys. Rev. B 48, 2365 (1993); Phys. Rev. B 51, 2268 (1995).
[10] N. Kim, G. Ihm, H.-S. Sim, and K. J. Chang, Phys. Rev. B 60, 8767 (1999).
[11] Y. Takagaki and D. K. Ferry, Phys. Rev B. 48, 8152 (1993).
[12] R. Garibay-Alomso, J. L. Marin and R. A. Rosas, Solid States Commun. 137, 248 (2006).
[13] W.-C. Tan and J. C. Inkson, Phys. Rev. B 53, 6947 (1996).
[14] U. Merkt, J. Huser, and M. Wagner, Phys. Rev. B 43, 7320 (1991); M.Wagner, U. Merkt, and A.V. Chaplik, *ibid* 45, 1951 (1992).